MICRO–SCALE MODELLING OF THE INTERACTION OF A PENETRATOR WITH A GRANULAR MEDIUM

K. Seweryn*†, J. Grygorczuk‡, M. Banaszkiewicz§

Abstract

The work presented in this paper is focused on the low velocity penetrator dynamics as the penetrator is driven into a granular medium. Surface and subsurface material of planets, comets and asteroids often consists of granular matter with grain sizes in the range from about μm to mm, like terrestrial sand. Theoretical approaches addressed to such systems (penetrator + medium) can be roughly divided into three categories: (i) microscopic models and molecular dynamics simulations, (ii) statistical mechanics and kinetic theory and (iii) continuum and phenomenological models. The molecular dynamics model (MD model) has been chosen to simulate the complicated dynamic interactions between each individual particle in the container and the surface of the penetrator. One of the objectives of this paper is to identify the optimal shape of the penetrator's tip during the stepped motion into a granular medium. Several simulations have been made assuming different conical angles of the tip from 120° to 30°. In addition, the dependency of the depth of penetration on the curvature of the conic section has been verified. A second objective, even more important, is to present the molecular dynamics (MD) method applied to modelling the dynamic behavior of the mole penetrator in a dense granular medium like quartz sand or gravel.

1 Introduction

The "mole" penetrometer is an axially symmetric intrusion device, which can move under the surface, discover the properties of the subsurface medium, sample the material, and in some cases, even return to the surface (Gromov et al., 1997; Kochan et al., 2001; Lorenz and Ball, 2001). The mole penetrator can be treated as a transport device for different sensors designed for *in situ* investigations in subsurface environments (Banaszkiewicz et

* *Space Research Centre, Polish Academy of Sciences, Bartycka 18 A, 00-716 Warsaw, Poland*
† *kseweryn@cbk.waw.pl*
‡ *jurekgry@cbk.waw.pl*
§ *marekb@cbk.waw.pl*

al. 2007; Dabrowski and Banaszkiewicz, 2006; Seweryn and Grygorczuk, 2006). The mole is driven by a hammering mechanism which accumulates energy in a spring and allows the mole to move forward by directed internal shocks. Over the recent years, several mole penetrators have been designed and tested in the laboratory. Some of them were prepared for a space mission. One was developed by DLR in Cologne and was used on the ill–fated *Beagle–2* lander aboard the ESA *Mars Express* mission (Coste, 1998; Richter, et al. 2002). Another interesting example is the HP^3 instrument proposed by DLR Berlin for the *ExoMars* mission (Knollenberg et al., 2007).

The budget restriction of mass and energy on a space instrument requires detailed investigation of the dynamic properties of the penetrator. The mole is a very good example of an instrument where mechanical and dynamic properties play an important role and should be optimized. In contrast to the standard penetrator, where the driving depth is limited by the length of the sensor rod (Seweryn et al., 2005; Spohn et al., 2007), the mole's depth of penetration is limited only by coupled dynamic properties of the mole and the surrounding medium (Richter et al., 2006) and by the length of the trailing tether. In other words, the mole concept is very useful to bring various sensors to deep subsurface layers and to measure physical properties and chemical composition of these layers. One of the properties of the mole that can be improved is the shape of the tip. In this paper, a method to obtain the optimal conical shape of the penetrator tip is presented.

In the last few years there have been many theoretical and experimental studies of surface properties of comet and asteroid bodies (Britt et al., 2002; Brownlee et al., 2004; Gaffey et al., 1993, 2002; Harris et al., 2005; Kömle et al., 2001). Many of them characterize surface material as a granular or foam–like matter. Colangeli et al. (1999) and Weissman et al. (2004) give the range of size distribution, grain shape and physical properties of the comet material. Gaffey et al. (1993, 2002) present a detailed investigation of the wide range of asteroids and provide information on their mineralogical characteristics. Many papers and experiments have focused on the Martian regolith properties (Arvidson et al., 2004; Moore et al., 1999; Ruff and Christensen, 2002; Squyres et al., 2006). In the last few years the Moon has been a target of numerous scientific theoretical and experimental considerations (Hill et al., 2007 and references therein). Lunar regolith is composed of particles that were derived either from lunar bedrock or from older regolith, which was formed when repeated meteoroid impacts pulverized the lunar bedrock, over–turning and mixing it, until it became a fine powder. Particles are heterogeneously mixed, and can range in size from microscopic to several meters or more in diameter, averaging between 60 and 110 μm (Willman et al., 1995).

Granular materials are systems of a large number of grains of various size, shape, and material properties. The motion of each particle is defined by Newtonian mechanics and contact mechanics of elastic and plastic deformation (Aranson and Tsimring, 2006). Although the interaction between two particles is simple, the behavior of the whole system is far from being understood completely (Hermann et al., 2001). The reason is that the dynamics of granular material are highly dissipative, the behavior of the medium depends on shear stresses, and in consequence the medium can be treated as a liquid or solid body (Volfson et al., 2003). The behavior of a granular medium is determined by the contact properties between the particles, i.e. Young's modulus and damping coefficient (Ciamarra

et al., 2004; Hermann et al., 1998). To describe the collective behaviour of a granular medium, the particle properties and interaction laws must be inserted into a discrete molecular dynamics scheme (Craig, 1997; Luding, 2004). From particle simulation one can extract many physical properties including, for example, the pressure of the system as a function of density, stresses, etc. (Luding, et al. 2001). The ODE equation of all particles allows a macroscopic description of the material which can be described as a compressible non–Newtonian complex fluid including fluid solid transition (Eggers and Riecke, 1998; Volfson et al. 2003). A crucial role in our MD simulation plays the penetrator shape, which in this study is modelled as a prism (Figure 1). In similar MD simulations the corresponding object is named a polygon or composite particle (Pöschel and Buchholtz, 1995). The penetrator dynamics depends both on properties of the medium and on those of penetrator itself, therefore a multi–parameter study is necessary to understand it. However, in this paper we have focused on a single parameter, i.e. the penetrator conical angle α (Figure 1) that we intended to optimize in order to get the best penetration progress.

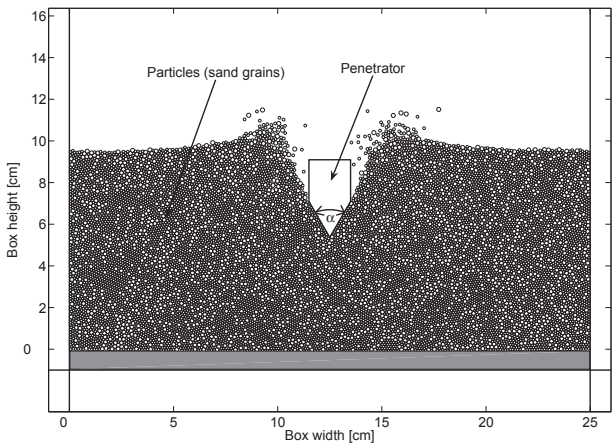

Figure 1: Molecular dynamics representation of a granular medium and penetrator tip with conical angle α.

The paper is organized as follows. First, we present a short theoretical description of the MD simulation assumptions and restrictions. In the next section we give a set of simple simulations to find out the overall characteristics of the system: elastic and damping parameters of the granular medium boundary and initial conditions etc. In this section, comparisons of our results with those obtained by Ciamarra et al. (2004) are provided to validate our model. The fourth section includes all results from the simulations. Finally, conclusions and future work directions are presented.

2 Theoretical considerations

There exist three fundamentally different approaches to describe the dynamics of a granular medium: (i) the so–called soft particles simulation method, (ii) the event–driven algorithm and (iii) the contact dynamics method for rigid particles (Aranson and Tsimring, 2006; Luding, 2004; Pöschel and Schwager, 2005; Rapaport, 2004). Although in general the event driven algorithm is much faster, our simulation was made using the soft particle algorithm, which is more suitable for dense granular material. The soft particle method uses the original model proposed by Cundal and Strack (1979). The method is based on a Lagrangian formulation which assumes that particle position, orientation, translational and angular velocity are independent variables. For this purpose, explicit expressions should be evaluated for all forces acting between all particles in contact. Since the deformation is associated with a change of particle shape (as determined by FEA explicit model), this poses a computationally big problem for a computer. However, the deformation may be approximated by an overlap area of the particles pressed against each other. Thus, the contact force F_{ij} acts between the two particles i and j in the point C and can be represented as sum of the elastic forces between them, which depend on the overlapping geometry and on the viscous forces (which in turn depend on the relative velocity between the particles (see Luding, 2004):

$$\vec{F}_{ij} \sim k \cdot \delta + \eta \cdot \vec{v} \tag{1}$$

Here k is proportional to Young's modulus, η is the damping coefficient and v is the relative velocity. The overlap δ is defined as the difference of the distance between the centers of mass of the two particles and the sum of their radii $r_i + r_j$ (Figure 2). This value can only be negative. Otherwise there is no contact between the two particles.

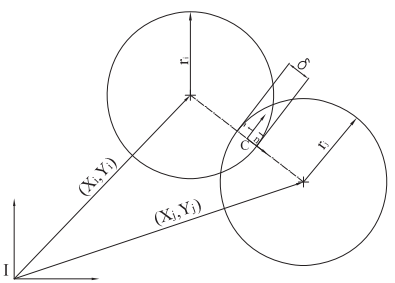

Figure 2: Schematic view of two particles during overlapping contact. The motion parameters are described in the inertial frame I, while the normal n and tangential t force components are calculated in the point C.

When decomposing a vector F into its normal and tangential components, the normal component is denoted as n and the tangential component as t. The unit normal vector

is defined by the line connecting the center of mass of the two particles (Džiugys and Bernhard, 2001). The origin of the non–moving laboratory coordinate system is located at point I. Assuming that $d << r_i$ the relative velocity of the contact point C in Figure 2 is defined as

$$v_{ij} = v_i + \omega_i \times r_i - (v_j + \omega_j \times r_j) \tag{2}$$

where the parameters indexed by i refer to the i'th particle's translational and rotational velocity. The same holds for particle j. The relative velocities (Eq. 2) can also be decomposed into normal and tangential components. Various models are used to calculate normal and tangential contact forces (linear Hookian contact law or Hertzian contact law) (Aranson and Tsimring, 2006; Leszczyński, 2003; Schwager and Pöschel, 2007). In this paper we apply Hook's law and therefore the normal component of the force has the form

$$F_n = k \cdot \delta + m_r \cdot \eta_n \cdot v_n \cdot \theta(v_n) \tag{3}$$

where m_r is the reduced mass of the two particles and θ is a Heaviside function to model elastic–plastic interactions (Labous and Rosato, 1997). The tangential forces act at the contact point. In absence of cohesion, Coulomb's law describes the coupling between the normal and tangential force $F_t \leq \mu \cdot F_n$,where μ is the friction coefficient. In short notation, the tangential contact law reads:

$$F_t = \min(\mu \cdot F_n, m_r \cdot \eta_r \cdot v_t) \tag{4}$$

where min follows the selection procedure described in the detail in Luding (2004). The parameters of motion are defined in the normal and tangential components at the contact point, then converted to an inertial frame and summed over each individual particle according the following averaging procedure (Luding et al., 2001)

$$F_i = \frac{1}{V} \sum_{p \in V} w_f \cdot V_p \sum_{c=1}^{Cp} F_{ic} \tag{5}$$

in which the inner summation is over all forces acting at the contact points, and next over all particles in an arbitrary volume. This averaging procedure can be formalized for any quantity, for example the stresses in the medium.

The problem of grain shape was discussed in detail in Džiugys and Bernhard (2001) and the references therein. Real grains can be represented in a 3D model by spheres, ellipsoids, polyhedrons, or in 2D by disks, ellipses or polygons. The main problem with a non spherical shape is to detect the contact with a neighboring particle and then calculating the overlap area, and the relative velocity in normal and tangential directions. For some analytical shapes, direct solutions can be found. However, a considerable computational expenditure is required for shapes that are more complicated. The most popular shape of particles is a sphere for 3D (Bougie, et al. 2002; Hermann and Luding, 1998; Hermann

et al., 2001) and a disk for 2D (Ciamarra et al., 2004; Volfson et al., 2003) models. The polygon particle shape is also a popular way to describe a medium with a large number of particles and sometimes allows one to reproduce the static friction better than the conventional model. (Pöschel and Buchholtz, 1995). In the soft particle algorithm, all forces acting on a particle either from walls or from other particles or external forces are calculated based on the positions of the particles. Once the forces are found, time is advanced by explicit integration of the corresponding Newtonian equations of motion (Dormand and Prince, 1980). Translational motion of the center of gravity of a particle i can be described by a system of Newton's equations

$$\frac{d\vec{X}_i}{dt} = \vec{V}_i \tag{6}$$

$$\frac{d\vec{V}_i}{dt} = \vec{a}_i \tag{7}$$

where the vectors X_i , V_i and a_i are position, velocity and acceleration of the center of gravity m_i of particle i. For a 2D system $\vec{X}_i \in (x_i, y_i)$, $\vec{V}_i \in (v_{xi}, v_{yi})$ and $\vec{a}_i \in (a_{xi}, a_{yi})$. Assuming that the i'th particle ($i \in (1, N)$, where N is total number of particles) is rigid, the vector F is the sum of all forces acting on the particle. Rotational motion of the particle i in the two dimensional case is describe by a Newton–Euler equation of the form

$$I_i \cdot \frac{d\omega_i}{dt} = T_i \tag{8}$$

where I is the general inertia tensor (in a 2 dimensional simulation, it is a scalar), ω is the angular velocity and T_i is the torque. By definition, the torque T is the summation of torques caused by the contact forces between the particles and can be written analogous to (Eq. 5) by substituting $F_{ic} = T_{ic}$, where $T_{ic} = r_i \times F_{ic}$. The equation of rotational motion in the 3D–simulation is much more complicated, it needs the full rank of the inertia tensor and requires that the computation should be done in a body–fixed frame. More detailed of information about rotational motion in free space can be found in Wertz (1978).

The properties of granular flow are dependent on the boundary conditions at the wall (Thompson and Grest, 1991). Often the proper boundary condition can determine the behavior of the system. Several types of boundary conditions can be used: (i) walls, which may be moving or stationary, (ii) inflow and outflow conditions and (iii) periodic conditions. The first two are clear and are well defined in many papers, but the last one is slightly tricky for its potential use in an MD simulation. If a macroscopic system can be described as periodic, then a small but finite system of periodic characteristic length scale dimensions can be extracted. Thus, the simulation of the small system represents the macroscopic behavior with sufficient accuracy. Periodic boundary conditions are necessary when the small system has the same conditions on the corresponding boundaries. For example, particles moving out at one edge of the container enter at the opposite edge with the same dynamic parameters (Džiugys and Bernhard, 2001). The contact duration is also of practical technical importance because the integration of the equation of motion

is stable only if the integration time step of the numerical scheme used (e.g. Runge–Kutta procedure) is smaller than the typical response time of the harmonic oscillator, which is given as

$$t_c = \frac{\pi}{\sqrt{\frac{k}{m} + \eta^2}} \tag{9}$$

Various time integration schemes can be used to solve Eqs. (6), (7), (8) (Dormand and Prince, 1980).

3 Description of the model

3.1 Model validation

This section is devoted to comparison and validation of the numerical code prepared to perform a numerical simulation based on the theory outlined above. As a guiding document we choose the paper of Ciamarra et al. (2004), in which the authors focused on the time evolution of a projectile's motion during impacting a granular material composed of individual discs. They compared experiments and numerical simulations on a two dimensional granular medium that yielded the time dependence of the drag force on the projectile. Following them we perform the same molecular dynamics simulation with a disc particle (radius $R = 2.23$ cm and mass $M = 32.2$ g) dropped into a bed of small particles (discs). The impact velocity of the particle was 3.6 m/s parallel to the gravity vector. To reduce crystallization, two sizes of small particles were used: 12600 small particles ($R = 0.228$ cm, $M = 0.049$ g) and 2400 bigger particles ($R = 0.316$ cm, $M = 0.097$ g). The particles were uniformly distributed in the container and initially pre–stressed. All model parameters, boundary conditions etc. were taken from Ciamarra et al. (2004) with the exception of the simulation step which in our case is 3 times larger (i.e. 3 μs instead of 1 μs). Figure 3B presents a screen shot from the simulation at 0.08 s. The comparison between experimental results and the simulation is presented in Figure 3A. The time evolution of position and velocity clearly shows that our model is consistent with the experiment.

3.2 Molecular dynamics simulation of sand

The shape of the test container with sand is cylindrical and its dimensions (radius 30 cm and height about 1 m) were chosen to minimize the influence of the walls on the penetrator motion (Figure 4A). The number of sand grains (all have a radius of about 0.25 mm) in such a container is about 10^8 and it is impossible to build and simulate such a big system, because of the high computational costs involved. Therefore several simplifications of the MD simulations were done to decrease the number of particles — all of these assumptions are summarized in Table 1.

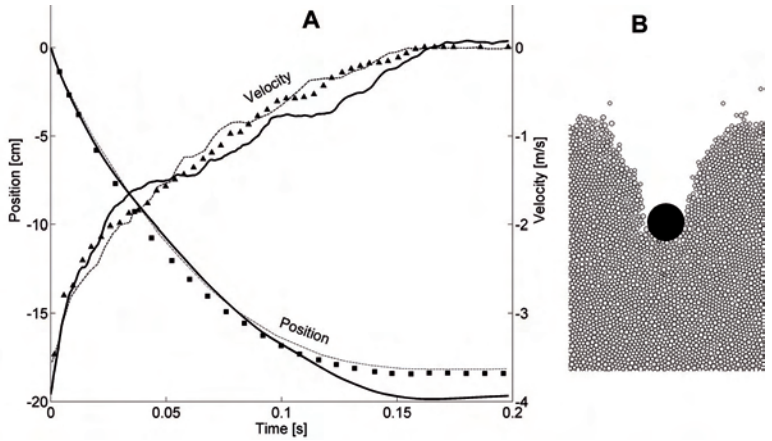

Figure 3: Comparison between our MD–simulations and the results obtained by Ciamarra et al. (2004). Panel B present a snapshot from the simulation. In panel A the position (left axis) and the velocity (right axis) of the particle during motion are shown: for experiments (square points); for Ciamarra et al. (2004) simulation results (dotted line), and for our simulation results (solid line).

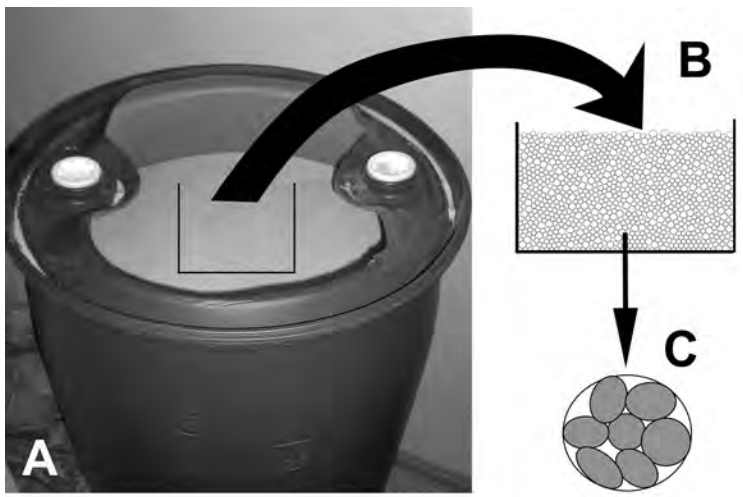

Figure 4: Schematic representation of simplifying assumptions used in simulations: the testbed system (A) is represented as a two–dimensional box (B) with particles composed of real sand grains (C).

First of all we consider a two–dimensional box (25 cm width and 10 cm height), see Figure 4B) with 2D disc–shaped particles which have the mass properties corresponding to the equivalent mass in a 3D system. Each regular disk represents the composite particle consisting of seven glued irregular grains (six particles around center one, see Figure 4C). A similar approach was described in (Hirshfeld et al., 1997; Pöschel and Buchholtz, 1993). Moreover, this assumption allows us to reduce the original Young's modulus of sand grains from 3×10^{10} (Cohen et al., 1994) to 10^3–10^4, which is unrealistically low. But the success of other MD simulations with reduced Young's modulus (Rapaport, 2002), despite this flaw, captures much of the dissipative dynamics. If the grains were regular and single–sized, the whole system would behave like a crystal, therefore two sizes of discs were used ($R_1 = 0.6$ mm, $M_1 = 0.022$ g; $R_2 = 0.9$ mm, $M_2 = 0.05$ g) to avoid such crystallization effects.

Table 1: Summary of the simulation model simplifications.

	Testbed system (A)	*Simulation box (B)*	*Composite particles (C)*
No. of particles	10^8	10^5	10^4
Dimension	3D	2D	2D
Shape	oval, ellipsoid	elliptical	cylindrical
Size distribution	Supplier data sheet	Not defined	two size of particles
Simulation time steps	10^{-8} s	10^{-8} s	10^{-4} s

In the next set of models, we have tried to find appropriate values of the model constants (k, η_n, η_t, etc.). Since we do not have a real mole penetrator yet, we made simple experiments with a steel sphere ($R_s = 12.2$ mm and $M_s = 11.2$ g), falling down with a velocity of 3.6 m/s (this corresponds to the 0.65 m height) and impacting the sand surface. The measured depth of penetration was 22 ± 1 mm and this value was the main fitting criterion (Figure 5). Moreover, we have tried to measure the velocity profile of the impacting projectile using a simple, low cost optical device. The results were not accurate enough, and only the qualitative behavior of the system was recorded, i.e. the small backward motion at the end of the experiment (Figure 5). Although no formal fitting method has been applied, the final results justify such a simplistic approach. The main lessons learned from the attempted fitting concern physics of the granular medium in a complicated system rather than mathematical estimates of the quality of the fit. Such a rigorous approach was nevertheless excluded because of too high computational costs (a single run takes about 30 h of CPU on a 2 processors AMD opteron 1.6 GHz computer with 3 Gb memory).

The molecular dynamics simulation of the sand contains 15 000 discs. Any two of them exert normal (Eq. 3) and tangential (Eq. 4) forces on one another with the following constants: $k = 10^3$ (proportional to Young's modulus), $\eta_n = 10^4$, $\eta_t = 8 \times 10^3$ (viscoelastic constants), and $\mu = 0.674$ is the static friction coefficient (Craig, 1997). The reduced mass m_r is defined as $m_r^{-1} = m_A^{-1} + m_B^{-1}$ for the two particles A and B. Following Ciamarra et al. (2004) we use the Heaviside function to simulate an elastic–plastic interaction. According to the simulations of a dense medium presented by Lee and Herrmann (1993)

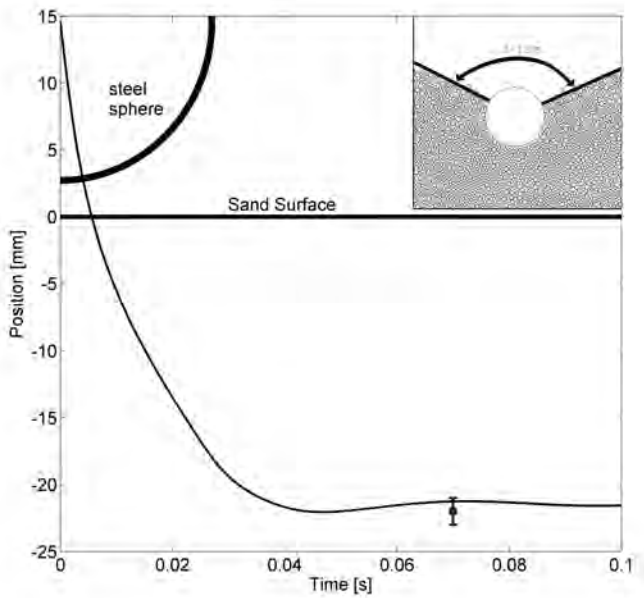

Figure 5: The position profile of the steel ball during impact into sand obtained for the best fitted simulation parameters (k, η_n, η_t). The single measurements (with RMS bar) of the final penetration depth agree well with the simulation results. The ball and the sand surface are schematically presented. Inset: angle of repose β obtained from MD simulation.

and by Taguchi (1992), we neglect the equation of rotational motion (Eq. 8) and therefore the relative velocity (Eq. 2) has the simpler form $v_{rel} = v_j - v_i$.

The key issue in solving the MD system is to define appropriate boundary conditions, especially when the simulation should reflect the behavior of a huge system by a relatively small number of particles. Since our system is symmetric to the x–component of the initial position of the penetrator, we use a periodic boundary condition to the left and right wall (Figure 4B) (Ristow et al., 1997). The boundary at the virtual bottom wall needs special consideration. The series of simulations clearly show that we cannot use a typical wall boundary condition because the time of wave propagation from the penetrator to the bottom and back (~ 0.03 s) is shorter than the time of the penetrator motion (~ 0.05 s). Therefore, we assume that the bottom wall should damp the motion of the particle near the boundary exponentially with time (Figure 6).

Mathematically, one can cast boundary conditions in the following form:

$$F_{n\_boundary} = (k \cdot \delta + m_r \cdot \eta_n \cdot v_n) \cdot \theta(v_n) \tag{10}$$

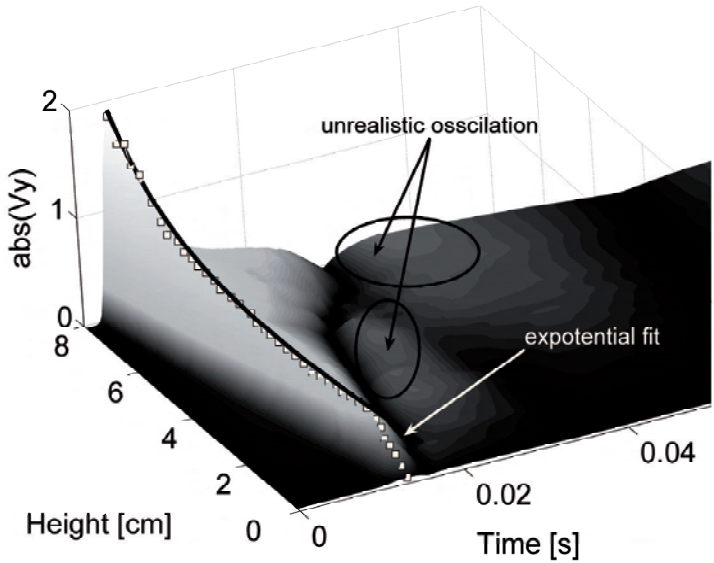

Figure 6: The 3D plot illustrates the time evolution (Y–axis) of the medium vertical velocity (Z–axis) as a function of depth below the penetrator (X–axis). The gray intensity represents the magnitude of the vertical component of velocity (white color correspond to the highest value). The square points correspond to the maximum velocity below the penetrator. The black line represents the exponential fit.

where $k = 1$, and the rest of the parameters are standard. It is important to note that the normal force exerted by the wall to the particle is zero when the velocity of the particle is positive. The effect of the application of such a boundary condition is shown in Figure 7, where the top panel correspond to the behavior of the system with a standard boundary condition, and the bottom one to case described by (Eq. 10). The particular curves in both panels corresponds to the vertical component of the velocity vector in equally spaced points below the penetrator (ee Figure 3). When we use boundary condition described by (Eq. 10), the lower boundary layer of the discs does not oscillate and therefore does not disturb the dynamics of whole system.

Another issue is to define proper initial conditions of the system. First, the static position of each disc has to be defined according to the original scheme, which places the discs one after another at minimum height and with zero velocity. Since the initial contact force between the discs cannot be specified a priori, the calculations were carried to the moment when the energy of the system was constant. In contrast to the matrix scheme presented by Džiugys and Bernhard (2001) our ideas allow us to decrease the time needed to obtain stable initial position.

The tip of the penetrator was modelled as a polygon shape particle (Pöschel and Buchholtz, 1995), see Figure 1), where the width and base height of the tip was 20 mm. The

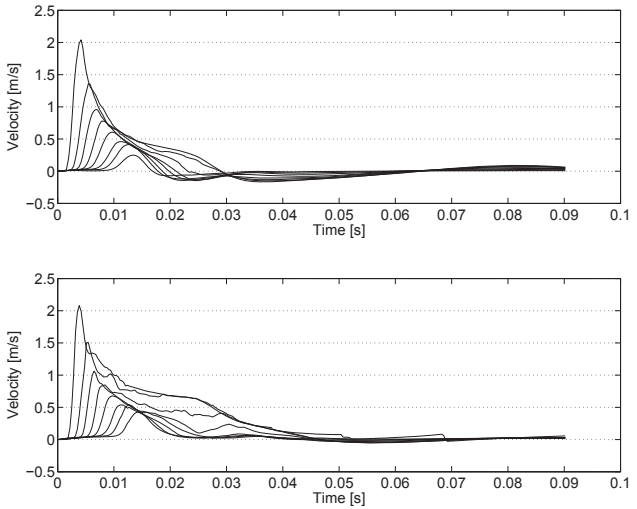

Figure 7: Velocity profiles of the medium in equally distributed points under the penetrator. The curves correspond to the smallest depths. The top panel corresponds to the standard wall boundary conditions, for which oscillations around zero velocity occur. The bottom panel corresponds to the boundary condition that suppresses oscillations.

conical opening angle α is the major parameter of the penetrator tip, and the presentation of how the dynamic properties depend on this angle is a major objective of this paper. The force exerted by the tip has the same form as the force between particles (Eq. 3 and 4), with the only difference being that the k parameters are two order of magnitude higher. The whole algorithm was coded in MATLAB software using a sparse matrix (Gilbert et al. 1992). The simulation uses a fourth order Runge–Kutta algorithm with a fixed time step of 30 μs which is smaller than the time of impact from (Eq. 9).

4 Results

All simulations started with the same initial conditions described in the previous section and were performed for the following conical angles: 120°, 90°, 60°, 45°, 30°. In addition a simulation with a nonlinear conical shape (ogive–shaped tip) was performed. The advantage of a molecular dynamic simulation is, of course, that it opens up the possibility of obtain position, velocity, forces and other dynamical properties of the system at each point and at any time. The most interesting information, however, is the state of the system at selected points of time. Therefore, we first present the time evolution of the whole system (Figure 8); the first panel corresponds to the situation before impact (a), then the penetrator impacts into the sand (b), next penetration with almost constant

deceleration takes place (c and d), and finally the penetrator comes to rest in a certain depth and the crater formed collapses (f).

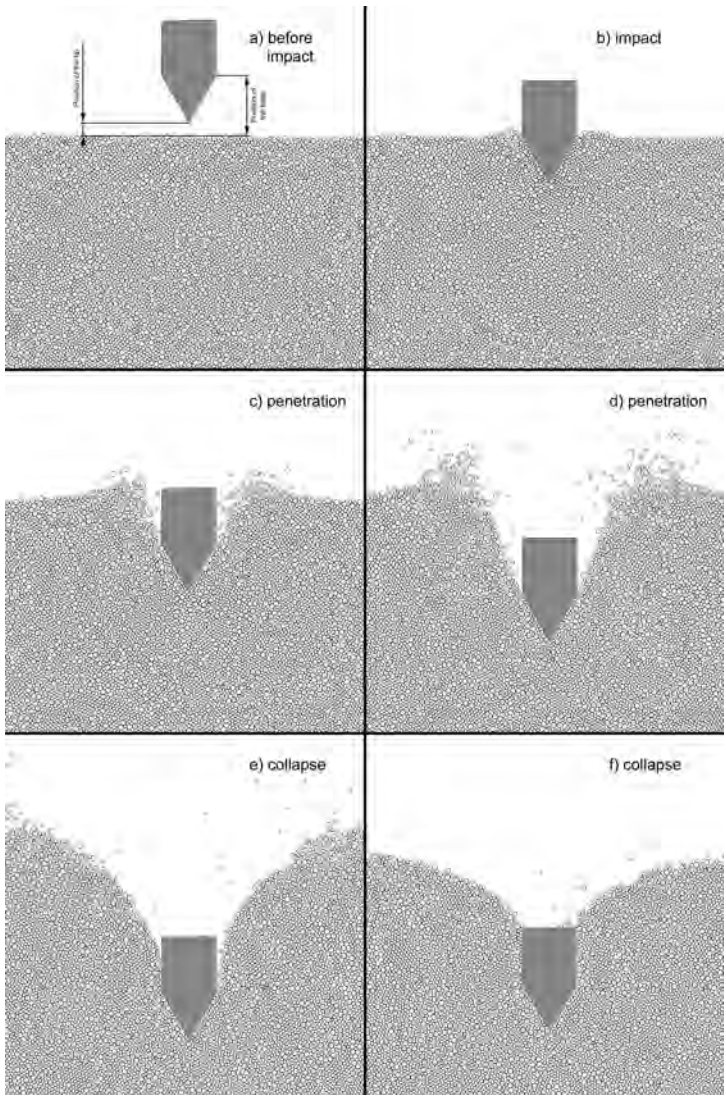

Figure 8: Snapshots of the penetrator motion for four different stages: before impact, during impact, during penetration and when the collapse occurs. In the first panel position of the tip and the base are indicated.

Figure 9 presents the velocity profile of the penetrator with different conical angles during penetration. One can see two interesting effects. The first one, that was expected, shows that a penetrator with a big conical angle, e.g. 120° (solid line) decelerates much faster than a penetrator with a small conical angle, e.g. 30° (dotted line). Second, qualitative differences between the MD simulation of the penetrator with the smallest and the one with the highest conical angle are observed. In some period the velocity of the penetrator with 30° conical angle changes linearly with time, but there is no such period for the penetrator with 120° conical angle. This effect is probably caused by acoustic waves which are excited in the latter case and which propagate vertically through the medium. Integration of the velocity gives the position of the penetrator in the granular medium. Note that Figure 10 represents position of the base of the penetrator (see Figure 8, first panel) which is a more valuable information than the position of the tip. The different initial positions of the penetrator are caused by different conical angles — the initial position of the tip for all cases are the same. The obtained final penetration depths are shown in Figure 11. Since the simulation box has dimensions of 20cm ×10cm, a molecular dynamics simulation of the penetrator with a small value of the conical angle (i.e. (10° or 20°) cannot be performed.

Finally, the dynamic properties of the penetrator with an ogive–shaped tip have been examined . In this case the axial cut of the tip shape forms part of a circle (see Figure 12). Initial and final angles were chosen as 25° and 45°. respectively. Such a configuration has been compared with the standard 25° and 45° conical angle penetrators. The obtained position of the base of the penetrator is presented in Figure 13. It is important to note that a penetrator with a circular shaped profile has almost the same dynamic properties as a 25° standard conical penetrator, but the length of the tip is 30% shorter.

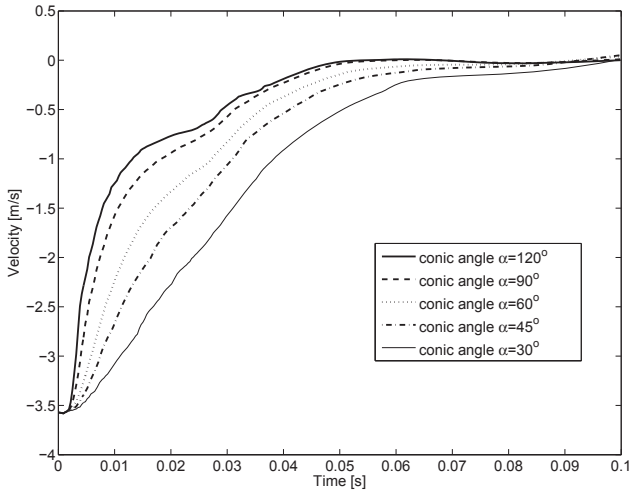

Figure 9: The velocity profiles of the penetrator tip for different conical angles α.

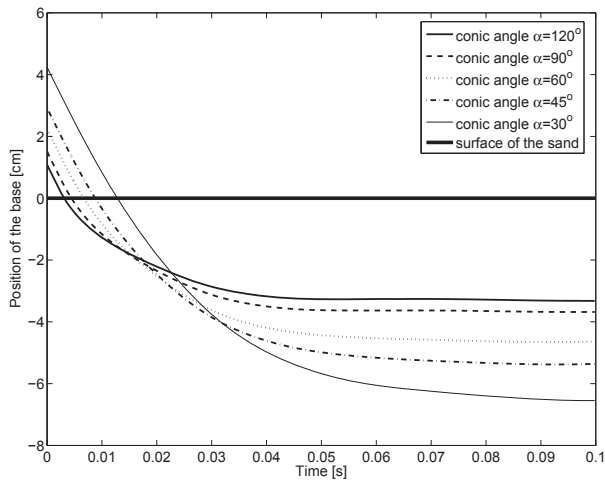

Figure 10: The position profiles of the penetrator tip for different conical angles α.

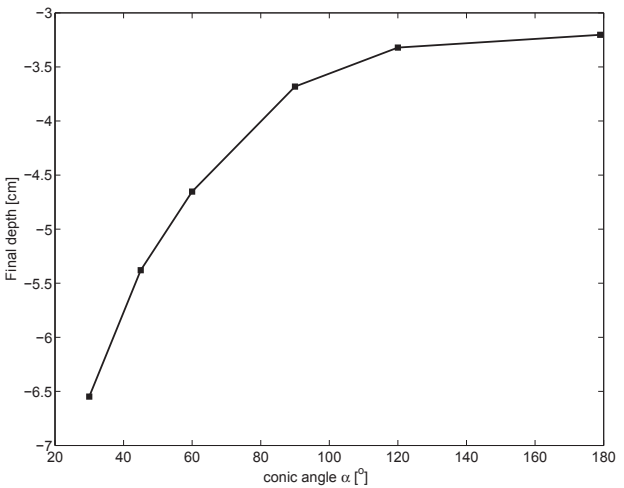

Figure 11: The final penetration depth for different conical angles.

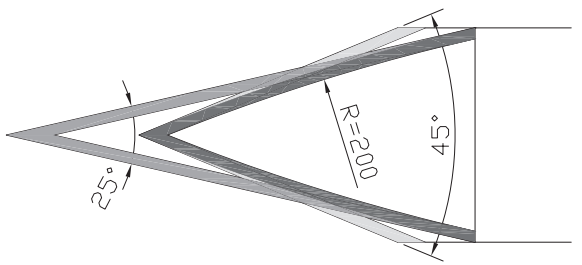

Figure 12: Geometry of three different penetrators tips; the one with 45° conical angle (bright line), the one with 25° conical angle (mid gray line) and the one one with a curved conical envelope (circular section with 200 mm radius of curvature) (dark line).

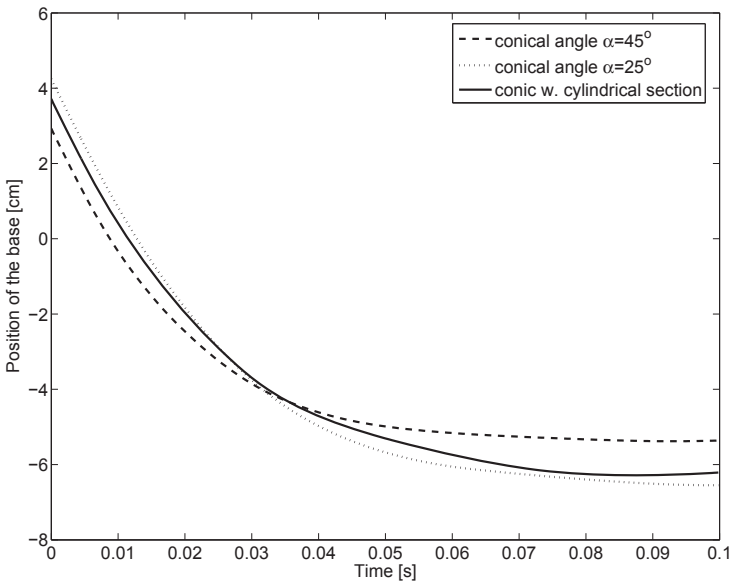

Figure 13: The penetration progress obtained for the tips presented in Figure 12. The dashed line corresponds to the 45° *conical angle penetrator, the dotted line to the* 25° *conical angle penetrator and the solid line corresponds to the ogive–shaped tip.*

5 Conclusions

The results of the performed molecular dynamic simulations in a granular medium can be summarized as follows:

a) The molecular dynamics simulation of the regolith was taken from Aranson and Tsimring (2006), Ciamarra et al. (2004), Džiugys and Bernhard (2001), Luding (2004) and then successfully applied to solve the problem of motion of a penetrator tip. However, as the method is computationally expensive, it is appropriate for a dense, highly dissipative and compressible medium. The paper presents the background elements of the MD simulation with application to penetrometry. In the future, the method will be extended using a parallel processing algorithm to solve the model with a higher amount of grains.

b) The paper presents a novel approach to simulate the boundary condition on the bottom wall, where the wave generated by collisions between penetrator and sand is almost perfectly damped. In this situation, the penetrator is not disturbed by the reflected wave and the number of particles can be limited to a value compatible with the available computational resources.

c) The results from the simulations of the standard conical penetrator tip clearly show that the depth of penetration depends on the conical angle of the penetrator tip and it increases with smaller angle. It is important to note that those results were obtained for simulations near the surface and that the dynamic behavior of a penetrator may change in the deeper regions of the regolith. Such a simulation will be performed in the near future.

d) For a high conic angle, the resisting force of the medium decreases for a short time period (Figure 9, solid line) and this fact can be used by the mole penetrator mechanism to get additional velocity and, in consequence, achieve a higher final depth.

e) The MD simulations confirmed that the curvature of the conical profile influences the penetrator dynamics. Since the initial conical angle is 45°, the strength and durability of the tip is much higher, especially in the case of penetration in gravel aggregate.

Future work will be focused on two different approaches towards the mole penetrator dynamics problem. Both of them are related to each other. However, the first one involves the simulation work i.e. coupled dynamics of the mole penetrator as a 3 mass system with the granular matter, the dynamic properties of the mole in the deeper region where these properties are crucial for them, and finally the full 3D simulation of the granular medium. The second one relies on the problem of validation of the MD simulation. In this paper, we compare the simulation results only with the simple drop tests. However, for the past 6 months, we have been developing a new mole penetrator which gives us the possibility to compare the results from the MD simulation with experimental results. The experience

gained with the previously successfully developed MUPUS penetrator, as well as the computer aided MD simulation gives us the possibility to determine the optimal design of the mole penetrator.

Acknowledgments

The authors are very grateful to B. Dabrowski, M. Strumik, M. Wachowicz, and R. Wawrzaszek for numerous discussions about the subject. The paper was partially supported from the KBN project No. N522 003 31/1166.

References

Aranson I.S., Tsimring, L.S.: Patterns and collective behavior in granular media: Theoretical concepts. *Reviews of Modern Physics* **78**, 641–692 (2006).

Arvidson R.E., Anderson R.C., Bartlett P. et al.: Localization and physical properties experiments conducted by Spirit at Gusev Crater. *Science* **305**, 821–824 (2004).

Banaszkiewicz M., Seweryn K., Wawrzaszek R.: A sensor to perform in–situ thermal conductivity determination of cometary and asteroid material. *Adv. Space Res.*, in press (2007).

Bougie J., Moon S.J., Swift J.B., et al.: Shocks in vertically oscillated granular layers. *Physical Review E* **66** 051301, (2002).

Britt D.T., Yeomans D., Housen K., et al.: Asteroid Density, Porosity, and Structure. In: *Asteroids III*, (Eds. Bottke W. F., Paolicchi P., Binzel R. P. et al.), Univ. of Arizona Press, 485–500 (2002).

Brownlee D.E., Horz F., Newburn R.L.: Surface of young Jupiter Family Comet 81 P/Wild 2: View from the Stardust Spacecraft. *Science* **304**, 1764–1769 (2004).

Ciamarra M.C., Lara A.H., Lee A.T. et al.,: Dynamics of drag and force distributions for projectile impact in a granular medium, *Physical Review Letters* **92(19)**, 194301 (2004).

Cohen M.D., Goldman A., Chen W.-F.: The Role of silica fume in mortar: transition zone vs. bulk paste modification. *Cement and Concrete Research* **24**, 95–98 (1994).

Colangeli L., Mannella V., Brucato J.R. et al.: Characterization of cosmic materials in the laboratory. *Space Science Review* **90**, 341–354 (1999).

Coste P.: Mobile penetrometer ground tests. *Proceedings of ESA Workshop on Advanced Space Technologies for Robotics and Automation – ASTRA*, ESA/ESTEC, Noordwijk (1998).

Craig R.F.: Soil Mechanics. Sixth edition. E & FN Spon, pp. 376—401 (1997).

Cundall P.A., Strack O.D.L.: A discrete numerical model for granular assemblies. *Geotechnique* **29**, 47—65 (1979).

Dabrowski B., Banaszkiewicz M.: Measurement of Lunar and Martian regolith thermal properties using subsurface robotic teams. *Proceedings of ESA Workshop on Advanced Space Technologies for Robotics and Automation – ASTRA*, ESA/ESTEC, Noordwijk (2006).

Dormand J.R., P.J. Prince: A family of embedded Runge–Kutta formulae. *J. Comp. Appl. Math.* **6**, 19–26 (1980).

Džiugys A., Bernhard P.: An approach to simulate the motion of spherical and non–spherical fuel particles in combustion chambers. *Granular Matter* **3**, 231–265 (2001).

Eggers J., Riecke H.: A continuum description of vibrated sand. *Phys. Rev. E* **59**, 4476 (1999).

Gaffey M.J., Bell J.F., Brown R.H. et al.: Mineralogical variations within S–type asteroids class. *Icarus* **106**, 573–602, 1993.

Gaffey M.J., Cloutis E.A., Kelley M.S. et al.: Mineralogy of Asteroids. In: *Asteroids III* (Eds. Bottke W.F., Paolicchi P., Binzel R.P. et al.), Univ. of Arizona Press, pp 183–204 (2002).

Gilbert J.R., Moler C., Schreiber R.: Sparse Matrices in MATLAB: Design and Implementation. *SIAM J. Matrix Anal. Appl.* **13**, 333–356 (1992).

Goldenberg C., Goldhirsch I.: Small and large scale granular statics. *Granular Matter* **6**, 87—96 (2004).

Gromov V.V., Miskevich A.V., Yudkin E.N. et al.: The Mobile Penetrometer - A "Mole" for sub-surface soil investigation. *Proceedings of the* 7^{th} *European Space Mechanisms & Tribology Symposium*, ESTEC, Noordwijk, The Netherlands, ESA SP–410 (1997).

Harris A.W., Meuller M., Delbó M. et al.: The surface properties of small asteroids: Peculiar Betulia—A case study. *Icarus* **179**, 95—108 (2005).

Hermann H.J., Luding S.: Modeling granular media on computer. *Contiuum Mech. Thermodyn.* **10**, 189—231 (1998).

Hermann H.J., Luding S., Cafiero R.: Dynamics of granular systems. *Physica A* **295**, 93—100 (2001).

Hill E., Mellin M.J., Deane B. et al.: Apollo sample 70051 and high- and low-Ti lunar soil simulants MLS-1A and JSC-1A: Implications for future lunar exploration. *J. Geophys. Res.* **112**(E2), doi:10.1029/2006JE002767 (2007).

Hirshfeld D., Radzyner Y., Rapaport C.: Molecular dynamics studies of granular flow through an aperture. *Physical Review E* **56**, 4404—4415 (1997).

Knollenberg J., Nadalini R., Spohn T.: Thermal measurements with HP3/TEM on ExoMars. EGU, Vienna (2007).

Kochan H., Hamacher H., Richter L.: The mobile penetrometer (Mole): A tool for planetary sub–surface investigations. In: *Penetrometry in the Solar System* (Eds. Kömle N.I., Kargl G., Ball A.J., Lorenz R., Verlag der Österreichischen Akademie der Wissenshaften, Wien (2001).

Kömle N.I., Ball A. J., Kargl G. et al.: Impact penetrometry on a comet nucleus – interpretation of laboratory data using penetration models. *Planet. Space Sci.* **49**, 575–598 (2001).

Leszczyński J.S.: A discrete model of a two–particle contact applied to cohesive granular materials. *Granular Matter* **5**, 91—98 (2003).

Labous L., Rosato A.D.: Measurements of collisional properties of spheres using high-speed video analysis. *Phys. Rev. E* **56**, 5717–5725 (1997).

Lee J., Herrmann H.J.: Angle of repose and angle of marginal stability: Molecular dynamics of granular particles. *J. Phys. A* **26**, 373—383 (1993).

Lorenz R.D., Ball A.J.: Review of impact penetration tests and theories. In: *Penetrometry in the Solar System*, (Eds. Kömle N.I., Kargl G., Ball A.J., Lorenz R., Verlag der Österreichischen Akademie der Wissenschaften, Wien (2001).

Luding S., Latzel M., Volk W., et al.: From discrete Eelement simulation to a continuum model. *Computer Method in Applied Mechanics and Engineering* **191**, 21–28 (2001).

Luding S.: Molecular Dynamics Simulations of Granular Materials. In: The Physics of Granular Media (Eds. Hinrichsen H., Wolf D.E.), WILEY–VCH Verlag GmbH & Co.KgaA, Weinheim, pp. 299–324 (2004).

Moore H.J., Bickler D.B., Crisp J.A., et al.: Soil–like deposits observed by Sojourner, the Pathfinder rover. *J. Geophys. Res.* **104**(E4), 8729–8746 (1999).

Pöschel T. Buchholtz V.: Static friction phenomena in granular materials: Coulomb law versus particle geometry. *Physical Review Letters* **70**, 3963—3966 (1993).

Pöschel T. Buchholtz V.: Molecular dynamics of arbitrarily shaped granular particles. *Journal de physique* **5**, 1431-–1455 (1995).

Pöschel T., Schwager T.: *Computational Granular Dynamics: Models and Alghoritms*. Springer (2005).

Spohn T., Seiferlin K., Hagermann et al.: MUPUS — a thermal and mechanical properties probe for the Rosetta Lander PHILAE. *Space Sci. Rev.* **128** (2007).

Squyres S.W., Knoll A.H., Arvidson R.E. et al.: Two years at Meridiani Planum: Results from the Opportunity Rover. *Science* **313**, 1403–1407 (2006).

Rapaport D.C.: Simulational studies of axial granular segregation in a rotating cylinder. *Phys. Rev. E* **65**, 061306 (2002).

Rapaport D.C.: *The Art of Molecular Dynamics Simulations*. 2^{nd} edition, Cambridge University Press (2004).

Richter L., Coste P., Gromov V.V., et al.,: Development and testing of subsurface sampling devices for the Beagle–2 lander. *Planetary and Space Science* **50**, 903–913, (2002).

Richter L., Gromov V.V., Kochan H. et al.: The Planetary Underground Tool (PLUTO) Experiment on the Beagle–2 Mars Lander. *Sixth International Conference on Mars* (2003).

Richter L., Gromov V.V., Re E.: MSM — Mole with Sampling Mechanism. Final Report of ESTEC Contract No. 14233/00/NL/WK(SC) (2006).

Ristow G. H., Strassburger G., Rehberg I.: Phase diagram and scaling of granular materials under horizontal vibrations. *Physical Review Letters* **79**, 833—836 (1997).

Ruff S. W., Christensen P.R.: Bright and dark regions on Mars: Particle size and mineralogical characteristics based on Thermal Emission Spectrometer data. *J. Geophys. Res.* **107**(E12), 1–21 (2002).

Seweryn K., Banaskiewicz M., Grunwald M., et al.: Thermal model of the MUPUS penetrator. *Int. J. Heat and Mass Transfer* **48**, 3713–3721, 2005.

Seweryn K., Grygorczuk J.: Subsurface mole for future planetary missions. *Proceedings of the Workshop on Space Technologies*, Krakow (2006).

Schwager T., Pöschel T.: Coefficient of restitution and linear dashpot model revisited. submitted to *Granular Matter* (2007).

Taguchi Y.: New origin of a convective motion: Elastically induced convection in granular materials. *Physical Review Letters* **69(9)**, 1367—1370, 1992.

Thompson, P.A., Grest, G.S.: Granular flow: Friction and the dilatancy transition. *Physical Review Letters* **67**, 1751—1754 (1991).

Volfson D., Tsimring L.S., Aranson I.S.: Partially fluidized shear granular flows: Continuum theory and MD simulations, *Physical Review E* **68**, 021301 (2003).

Weissman P.R., Asphaug E., Lowry S.C.: Structure and Density of Cometary Nuclei. In: *Comets II* (Eds. M. Festou, H.U. Keller, and H.A Weaver), Univ. of Arizona Press, Tucson, pp. 337–357 (2004).

Wertz J.R.: *Spacecraft Attitude Determination and Control.* Dordrecht (1978).

Willman B.M., Boles W.W., McKay D.S. et al.: Properties of Lunar Soil Simulant JSC–1, *J. Aerosp. Engrg.* **8**, 77–87 (1995).